ADVANCED MATERIALS
www.advmat.de

Nanoscopic Patterned Materials with Tunable Dimensions via Atomic Layer Deposition on Block Copolymers

By *Qing Peng, Yu-Chih Tseng, Seth B. Darling,** and *Jeffrey W. Elam**

Patterned nanoscale inorganic materials with controllable characteristic feature size, symmetry, and properties are of considerable interest in a wide range of fields.[1–6] As dimensions proceed below 50 nm, top-down optical lithography patterning methods typically suffer from slow speeds and high costs. An alternative inexpensive approach is to mimic the biomineralization process[7–10] and use self-assembled organic structures as the growth-directing agents to guide the growth of inorganic materials into the desired morphology.[7–12] Block copolymers (BCPs), which have two or more chemically dissimilar homopolymers joined together through covalent bonds, can self-assemble into ordered periodic nanostructures (*e.g.* spheres, cylinders, lamellae, and bicontinuous structures)[6,13–15] under appropriate conditions due to microphase separation. BCPs offer an easy, inexpensive, and versatile platform for templating inorganic materials growth.[6,13–15] A variety of inorganic materials growth methods[6,11,13–24] have been applied onto the self-assembled BCPs for localized selective growth of materials in the desired domains, which act as nanoreactors to physically confine the growth, generally through hydrophobic forces.[11,18–24] Dimensions of templated materials, therefore, are determined by the physical size of the original domains in the BCP scaffold,[11,18–24] which limits the flexibility of these methods. Moreover, the loss of selectivity from uncontrolled homogeneous reactions cannot be fully prescribed, especially for reactions involving hydrolytic unstable precursors such as titania and other technologically important metal oxides.[11,14] Furthermore, the localized material growth in the targeted domains is not controllable on the molecular level,[6,11,13–24] which is important for assuring large-scale uniformity in mass production of organized nanoscale materials with controlled material properties.

In this work, the integration of atomic layer deposition (ALD)[25–31] with BCPs is presented as a solution, based on the principles of molecular recognition and organized assembly,[7–10] to address these challenges. In contrast to previous methods, this approach uses polymer chains in well-defined BCP domains as the molecular scaffold for templating materials growth through a controllable molecular assembly process. One common BCP system, polystyrene-*block*-poly(methyl methacrylate) (PS-*b*-PMMA, M_w = 50 500/20 900) is presented as an illustrative example, but this methodology can be extended via the virtually limitless variety of chemistries available both in BCPs and ALD. It involves two key steps. Selective and self-limited interaction of metal precursors such as $TiCl_4$, $AlCl_3$, $Al(CH_3)_3$, etc., which are Lewis acids, with carbonyl groups[32–35] in PMMA microdomains is used to generate nucleation sites along the polymer chains for the subsequent ALD processes.[25–31] The characteristic self-limited heterogeneous reaction feature of both steps, enables molecular level controllability in the process and, in principle, guarantees controllable macroscopic processing.[25–31] As a demonstration of this approach, organized Al_2O_3 and TiO_2 nanocylinders with controllable dimensions were synthesized.

Figure 1 shows the scheme for patterning inorganic nanoscale features onto the substrate by applying ALD onto a self-assembled PS-*b*-PMMA block copolymer film template. PS-*b*-PMMA samples (Figure 1a) are exposed to the vapor of metal precursors that diffuse into BCP films and react specifically with carbonyl groups in the PMMA domains. (Note that although carbonyl groups are used here as an example, a variety of different polymer units interacting with metal precursors through metal-ligand coordination, covalent bonding, and other interactions can also be used. For example, the pyridine groups in polyvinylpyridine, a common block for BCPs, could selectively bind metal compounds including $Al(CH_3)_3$, $AlCl_3$, $ZnCl_2$, $CdCl_2$, etc,[36] which are precursors for ALD processes. The hydroxyl groups in polyacrylic acid, another common block for BCPs, could react with $Al(CH_3)_3$, $TiCl_4$, and $Zn(C_2H_5)_2$ to form covalent bonds.) Non-coordinated excess metal precursors are then removed from the domains by a purge step with high purity N_2 to assure that reaction is self-limited and no homogeneous reaction occurs. The first monolayer of coordinated metal precursors provides reactive sites for the subsequent ALD, which selectively decorates the active PMMA domains (Figure 1b). As ALD operates in a self-limited heterogeneous surface reaction mode,[25–31] the growth of materials in the PMMA domains continues in bottom-up assembly fashion with molecular precision.[25–31] Finally, the polymer template in the composites is removed by thermal annealing or plasma treatment, leaving behind patterned inorganic materials that mimic the original self-assembled PMMA domains (Figure 1c). Because the assembly process in this technique uses units on the polymer chains as the molecular template, the final domain size of the inorganic material is mainly determined by a combination of the number of available reactive sites in the domain and the amount of material being assembled into the domain through ALD cycling, which offers unprecedented flexibility for tuning the final feature size compared with traditional methods,[11,16–24] including the fabrication of features considerably narrower than

[*] Dr. Q. Peng, Dr. J. W. Elam
Energy Systems Division
Argonne National Laboratory
Argonne, IL, 60439 (USA)
E-mail: jelam@anl.gov
Dr. Y.-C. Tseng, Dr. S. B. Darling
Center for Nanoscale Materials
Argonne National Laboratory
Argonne, IL, 60439 (USA)
E-mail: darling@anl.gov

DOI: 10.1002/adma.201002465

© 2010 WILEY-VCH Verlag GmbH & Co. KGaA, Weinheim

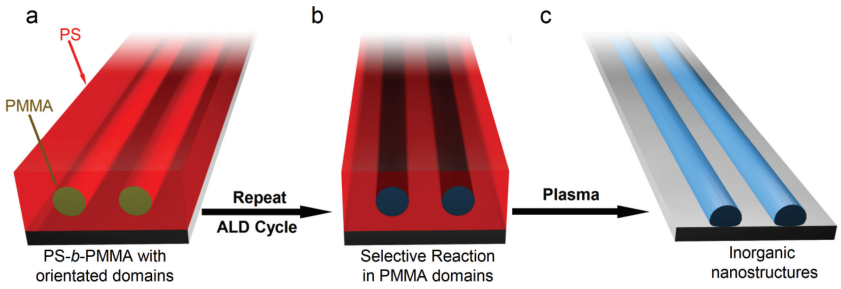

Figure 1. Schematic diagram for self-assembled PS-*b*-PMMA thin film templated synthesis of nanoscopic inorganic materials by ALD. a) Self-assembled PS-*b*-PMMA films b) Self-organized copolymer films are dried and then treated using ALD. Two key steps involved in the process, 1) Selective and self-limited coordination reaction between metal precursors and carbonyl groups in PMMA. 2) Selective and self-limited growth of materials by ALD with coordinated metal precursor as the nucleation site. c) Patterned inorganic material after the copolymer template is removed by thermal annealing or plasma treatment.

the template feature dimension. The separated heterogeneous surface reactions in this process greatly decrease the chance of uncontrollable overgrowth in undesired microdomains.[25–31] For simplicity, in the following test we refer to the first pulse of metal precursor and the following reactant dose as the first ALD cycle. The subsequent traditional ALD cycles of metal precursor/reactant are referred to as cycles 2, 3, 4, and so on.

Figure 2a–e are scanning electron microscopy (SEM) images of patterned Al_2O_3 nanocylinders resulting from 1, 2, 3, 6, and 10 cycles of Al_2O_3 ALD (timing sequence: 60/300/60/300 s), respectively, followed by O_2 plasma treatment. As presented in Figure 2a–e, each of Al_2O_3 stripe patterns resembles the parallel-oriented cylindrical microdomains of PMMA in the original PS-*b*-PMMA thin film (Figure S1 of the Supporting Information). The presence of Al was verified by energy dispersive X-ray (EDX) imaging (Figure S2). Contraction of the polymer and aggregation of the Al_2O_3 nuclei during the O_2 plasma etching process explain the formation of solid Al_2O_3 cylinders. The diameter of the Al_2O_3 cylinders resulting from one TMA/H_2O cycle is 8.48 ± 1.54 nm, which is much smaller than the ~30 nm-wide PMMA domains in the BCP films and much bigger than what one would expect from a traditional Al_2O_3 ALD on a planar surface (growth rate = 1.2 Å/cycle). According to the self-limiting reaction between TMA and carbonyl groups as illustrated in Scheme S1,[32] the cylinder diameter resulting from the first TMA/H_2O ALD cycle would be around 11.5 nm (see Supporting Information), which is slightly higher than the actual value we observed. We attribute the smaller measured size of the Al_2O_3 cylinders to the reduced number of coordinated TMA molecules by steric effects of ligands in TMA and the polymer substrate and folding of the polymer chains.[27–29] This mechanism is further supported by the broken points (as indicated by the arrows in Figure 2a) along the Al_2O_3 cylinders. More importantly, the smaller Al_2O_3 feature size than the theoretical value supports that the reaction of TMA in the PMMA domains is templated by the carbonyl groups on the polymer chain, and that the coordination process of TMA onto the carbonyls is indeed self-limited, which are vital for the proposed reaction processes to achieve molecular-level controllability.

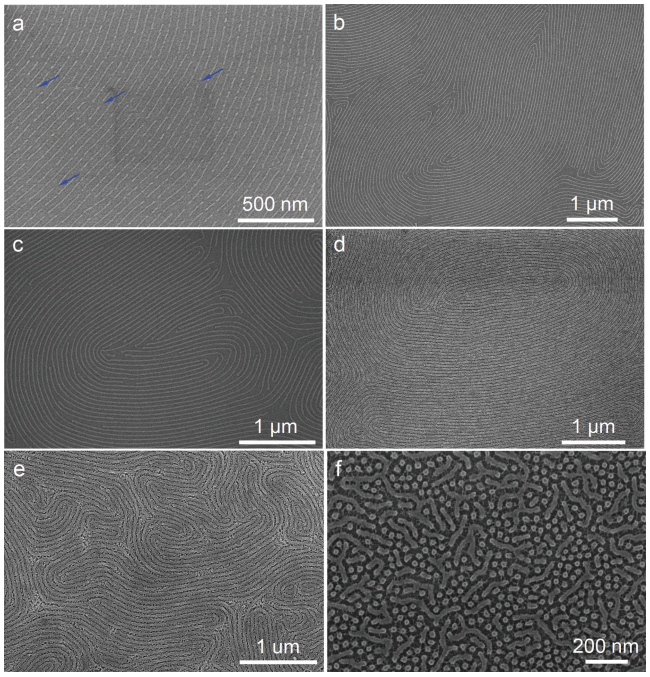

Figure 2. SEM images of Al_2O_3 patterns templated from PS-*b*-PMMA films on Si wafers after various numbers of ALD Al_2O_3 cycles with the timing sequence (60/300/60/300 s) followed by O_2 plasma treatment: (a) 1 cycle, (b) 2 cycles, (c) 3 cycles, (d, f) 6 cycles, (e) 10 cycles. Arrows in (a) indicate broken points along the cylinders. f) Mixture of Al_2O_3 nanoposts and nanocylinders.

The Al–OH species formed in the first ALD cycle through the coordination reaction between TMA and the carbonyl groups followed by H_2O hydrolysis served as nucleation sites for traditional Al_2O_3 ALD to incorporate more –Al–O ligands into the domains in a self-limited, layer-by-layer fashion. With increasing Al_2O_3 ALD cycles, the diameter of the Al_2O_3 cylinders increases as deduced from Figure 2a–e. After 10 ALD cycles, the diameter of the Al_2O_3 cylinders increases to 30.8 ± 2.7 nm, which is comparable with the original PMMA domain size. Moreover, the Al_2O_3 cylinders become continuous for samples with more than one TMA/H_2O ALD cycle as evidenced by the absence of visible breaks in Figure 2b–e. The cylinder diameters as well as the center-to-center spacings measured from the SEM images (Figure 2a–e) are plotted against the number of ALD cycles in **Figure 3**. The mean center-to-center value remains nearly constant (~60 nm) regardless of the number of ALD cycles performed. This value is consistent with the center-to-center spacing between PMMA domains in the initial BCP thin film template (60 nm ± 5 nm).

The capability of ALD to tune the feature size independent of the BCP template dimensions was highlighted by the linear dependence of the Al_2O_3 cylinder size on the number of ALD cycles (Figure 3). This eliminates the need to prepare BCPs with different domain sizes for synthesizing nanostructures of different sizes, therefore simplifying the process dramatically. This also supports that polymer chains represent the molecular

© 2010 WILEY-VCH Verlag GmbH & Co. KGaA, Weinheim

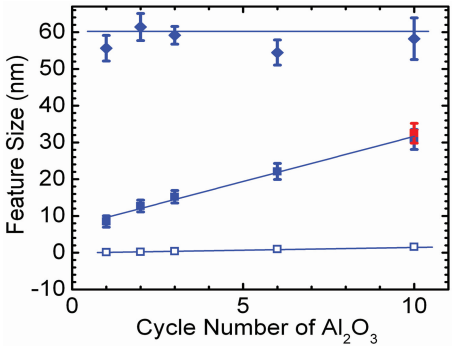

Figure 3. Diameter (■) and center-to-center spacing (♦) of Al_2O_3 cylinders as a function of ALD cycle number. The corresponding Al_2O_3 film thickness (□) on the Si witness substrates is included for comparison. All lines are guides for the eye. Red (■) indicates the size of the Al_2O_3 stripes generated from Al_2O_3 ALD with sequence timing (300/300/300/300 s).

templates for directing the localized growth of materials. Note that in Figure 3 the diameter of the Al_2O_3 cylinders from 10 ALD cycles using 5× larger precursor exposure times (timing: 300/300/300/300 s) is nearly the same as the cylinder diameter obtained using smaller precursor exposures. This demonstrates that Al_2O_3 ALD in the PMMA domains is indeed self-limited. This also suggests that the 60 s reactant exposures are close to the saturation point of the growth and 300 s purge times are sufficient to ensure self-limited growth. The slope of the line in Figure 3 yields an increase of ~2 nm/cycle, which is 16× higher than the Al_2O_3 ALD growth rate of 1.2 Å/cycle on planar surfaces determined by ellipsometry from the Si witness samples (lower trace in Figure 3). The higher growth rate on the polymer is ascribed to the higher density of accessible reactive sites on the permeable, three dimensional PMMA domains with respect to the solid, two dimensional flat Si surface. On the other hand, the growth rate of the Al_2O_3 cylinder diameter is smaller than the theoretical value (~10 nm/cycle) obtained by assuming that all Al–OH sites in the polymer matrix contribute to the Al_2O_3 ALD. This indicates that steric hindrance from the Al–OH and the polymer ligands limits the number of accessible Al–OH sites.

As the ALD cycles are repeated, rough material is observed in the PS domains after around 6 cycles (Figure S3a) which could be due to the nucleation of Al_2O_3 ALD on the PS domains and hence a decrease in selectivity. For the sample with 10 cycles of Al_2O_3 ALD, more Al_2O_3 growth was observed (Figure S3b). Due to the inert chemistry of PS to this particular ALD reaction scheme, nonselective Al_2O_3 ALD in the PS domains is likely the result of physical trapping of reactants, which might be reduced using longer ALD purge times.

In addition to the flexibility in material deposition, there is also flexibility regarding the morphology of the BCP template and, therefore, the ultimate inorganic nanostructures. For instance, when the PMMA domains are oriented normal to the substrate, Al_2O_3 nanoposts (Figure 2f) are formed with a diameter of 22.6 ± 2.8 nm similar to the in-plane cylinder diameter of 22 ± 2.2 nm observed elsewhere on the same sample. This phenomenon suggests that this process could be extended to synthesize nanomaterials with any of the morphologies accessible to BCPs, even into three dimensional matrices.

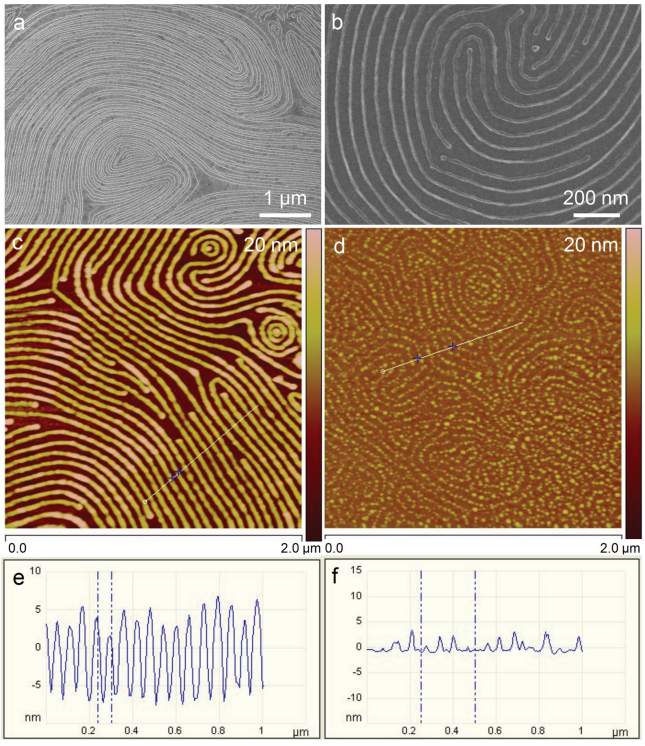

Figure 4. SEM images of TiO_2 aligned cylindrical pattern on Si wafer, formed by: a) 5 cycles TiO_2 ALD, and b) 10 cycles TiO_2 ALD. c) AFM height image of the pattern resulting from 10 cycles TiO_2 ALD on PS-*b*-PMMA thin film, d) AFM height image resulting from 1 cycle TiO_2 ALD. e) Line scan from Figure c. f) Line scan from Figure d. PS-*b*-PMMA was removed by O_2 plasma.

Analogous to the alumina process outlined above, this method is also applied to the preparation of patterned TiO_2 cylinders using TiO_2 ALD (timing sequence: 300/300/300/300 s) at 135 °C onto the PS-*b*-PMMA BCP thin films. In the first cycle, $TiCl_4$ coordinates to carbonyl groups as illustrated in Scheme S2,[33,34] and during the following half cycle H_2O hydrolyzes it to form Ti-OH. The Ti-OH species then serve as reactive sites for the subsequent $TiCl_4/H_2O$ ALD cycles. Organized patterns of TiO_2 cylinders generated with 5 cycles and 10 cycles of TiO_2 ALD are observable under SEM as shown by **Figure 4a** and 4b respectively. Atomic force microscope (AFM) measurement and the corresponding line scan (Figure 4c and Figure 4e) confirm the clear patterns of TiO_2 cylinders resulting from 10 cycles. No obvious pattern was observed by SEM for the sample after one cycle $TiCl_4/H_2O$, which may be due to the limited amount of coordinated $TiCl_4$. However, the AFM image and line scan for this sample (Figure 4d and 4f) do show TiO_2 pattern that follows the BCP template. X-ray photoelectron spectroscopy (XPS) measurement (Figure S4) confirms the presence of Ti on the sample surface. As shown in Figure 4a and 4b, the domains in light contrast are TiO_2 cylinders with diameters of 13.3 ± 1.4 nm and 16.9 ± 1.9 nm after 5 and 10 ALD TiO_2 cycles, respectively, are smaller than the size of the scaffolding PMMA domains (~30 nm) and again indicate that the TiO_2 growth is guided by the molecular template on the polymer chain. The center-to-center distances are nearly identical for these two

© 2010 WILEY-VCH Verlag GmbH & Co. KGaA, Weinheim

samples, which are 55.6 ± 6.6 nm and 59.3 ± 3.2 nm, respectively, which again match the corresponding spacing between the PMMA domains. These results confirm that the TiO_2 features preserve the original pattern present in the PS-*b*-PMMA thin film template. 10 cycles of TiO_2 ALD onto a PS-*b*-PMMA thin film were carried out at 85 °C as well. No patterned TiO_2 features were observed by SEM, which is probably due to the thermodynamically limited coordination reaction between the $TiCl_4$ and the carbonyl groups in the PMMA domains at this lower temperature.[35]

Our results establish a new method for the controllable preparation of patterned nanostructures of a broad variety of materials with tunable characteristic feature sizes and shapes by utilizing the confluence of unique capabilities inherent to atomic layer deposition, block copolymer self-assembly, and selective interaction of metal precursors with polymer units. Owing to the wide range of selective chemistries between metal precursors and polymer units and the enormous library of block copolymers and atomic layer deposition processes, patterned functional materials could be synthesized onto a broad range of substrates by carefully designing block copolymers and selecting ALD parameters.

Experimental Section

PS-*b*-PMMA (M_w = 50 500/20 900) was purchased from Polymer Source, Inc. and purified through Soxhlet extraction to remove excess PS homopolymer. BCP films were prepared by spin coating from a toluene solution (13 mg/mL) onto cleaned silicon substrates with native SiO_2. After deposition, films were annealed at 250 °C for two hours in a tube furnace under a flowing Ar atmosphere, then cooled down to room temperature in order to obtain self-assembled patterns. The in-plane PMMA cylinders are 30 ± 3 nm in diameter, and the center-to-center lateral distance is 60 ± 5 nm as illustrated in Figure S1. The thickness of a single-layer BCP film is around 60 nm. Most of the samples presented in this work have a single layer of cylindrical domains, though a few exhibit double layers.

ALD was performed in a custom viscous flow reactor as described previously.[37] The ALD reactants trimethyl aluminum ($Al(CH_3)_3$, TMA 96%) and titanium tetrachloride ($TiCl_4$, 99.9%), were purchased from Sigma-Aldrich and used as received. Deionized H_2O was generated from an on-site purifier. Ultrahigh purity N_2 (99.999%) was used as the purge gas and carrier gas with further purification by an inert gas filter (Aeronex Gatekeeper) before entering the reactor. Al_2O_3 and TiO_2 ALD were performed with alternating exposures to TMA/H_2O (at 85 °C) and $TiCl_4$/H_2O (at 85 and 135 ° C), respectively. All precursors were introduced into the ALD reactor as room temperature vapors. Si substrates with block copolymer coatings were loaded into the reactor on a stainless steel tray. In order to remove moisture and achieve thermal equilibrium, the samples were subjected to a 300 sccm N_2 flow at 1 Torr for at least 30 minutes and then evacuated to less than 20 mTorr before commencing ALD. The ALD was performed in a semi-static mode[38] as follows: Before the reactant exposure, the reaction chamber was first evacuated to ~20 mTorr. Next, 5 Torr of the first precursor was admitted into the reactor. After a predetermined exposure period, the excess reactants and byproducts were evacuated below 20 mTorr. The chamber was then purged with N_2 gas with flow rate of 300 sccm at 1 Torr for a predetermined period. The chamber was then evacuated again below 20 mTorr. The same evacuation-fill-purge-evacuation process was used for all reactants and repeated cyclically as in traditional ALD. The ALD timing sequence is given as: a/b/c/d where a and c are the exposure times to the metal precursor and the coreactant, respectively, and c and d are the corresponding purge times with all times given in seconds (s). To verify the absence of gas phase homogeneous reactions, a bare Si substrate with native oxide (cleaned by sonicating in acetone, flushing with isopropanol, and drying with nitrogen gas) was used as a witness substrate for each run.

The samples were characterized using a tapping-mode atomic force microscope (AFM, Veeco MultiMode V). The polymers were removed either by heating in air at 500 °C for 6 hrs or O_2 plasma etching performed at 50 W for 5 minutes in a March CS-1701 plasma etcher. A field emission scanning electron microscope (SEM, Hitachi S-4700-II) was used to examine the surface of the resulting materials after polymer removal. For the feature sizes deduced from the SEM images, mean values and corresponding standard deviations are reported from more than 50 measurements performed at different locations on the images. The SEM was equipped with an energy-dispersive X-ray (EDX) detector for elemental analysis. Spectroscopic ellipsometry (J. A. Woollam Co. Inc., alpha-SE) was used to evaluate the ALD film thickness on the silicon witness samples. X-ray fluorescence (XRF) analysis was carried out on an Oxford Instruments ED2000. X-ray photoelectron spectroscopy (XPS) was performed using MgKα (1253.6 eV) radiation and a hemispherical electron energy analyzer.

Supporting Information

Supporting Information is available from the Wiley Online Library or from the author.

Acknowledgements

Use of the Center for Nanoscale Materials was supported by the U.S. Department of Energy, Office of Science, Office of Basic Energy Sciences, under Contract No. DE-AC02–06CH11357. This work was supported in part by the Argonne-Northwestern Solar Energy Research Center, an Energy Frontier Research Center funded by the U.S. Department of Energy, Office of Science, Office of Basic Energy Sciences under Award Number DE-SC0001785.

Received: July 8, 2010
Published online: September 8, 2010

[1] G. K. Mor, O. K. Varghese, M. Paulose, K. Shankar, C. A. Grimes, *Solar Energy Materials and Solar Cells* **2006**, *90*, 2011.
[2] J. I. Martin, J. Nogues, K. Liu, J. L. Vicent, I. K. Schuller, *J. Magn. Magn. Mater.* **2003**, *256*, 449.
[3] C. L. Haynes, R. P. Van Duyne, *J. Phys. Chem. B* **2001**, *105*, 5599.
[4] N. L. Rosi, C. A. Mirkin, *Chem. Rev.* **2005**, *105*, 1547.
[5] J. V. Barth, G. Costantini, K. Kern, *Nature* **2005**, *437*, 671.
[6] H. C. Kim, S. M. Park, W. D. Hinsberg, *Chem. Rev.* **2010**, *110*, 146.
[7] S. I. Stupp, P. V. Braun, *Science* **1997**, *277*, 1242.
[8] G. M. Whitesides, J. P. Mathias, C. T. Seto, *Science* **1991**, *254*, 1312.
[9] S. Mann, G. A. Ozin, *Nature* **1996**, *382*, 313.
[10] I. A. Aksay, M. Trau, S. Manne, I. Honma, N. Yao, L. Zhou, P. Fenter, P. M. Eisenberger, S. M. Gruner, *Science* **1996**, *273*, 892.
[11] R. A. Pai, R. Humayun, M. T. Schulberg, A. Sengupta, J. N. Sun, J. J. Watkins, *Science* **2004**, *303*, 507.
[12] Y. Wan, D. Y. Zhao, *Chem. Rev.* **2007**, *107*, 2821.
[13] M. J. Fasolka, A. M. Mayes, *Ann. Rev. Mater. Res.* **2001**, *31*, 323.
[14] J. Bang, U. Jeong, D. Y. Ryu, T. P. Russell, C. J. Hawker, *Adv. Mater.* **2009**, *21*, 4769.
[15] S. B. Darling, *Prog. Polym. Sci.* **2007**, *32*, 1152.
[16] S. Horiuchi, T. Fujita, T. Hayakawa, Y. Nakao, *Langmuir* **2003**, *19*, 2963.
[17] S. Horiuchi, M. I. Sarwar, Y. Nakao, *Adv. Mater.* **2000**, *12*, 1507.

© 2010 WILEY-VCH Verlag GmbH & Co. KGaA, Weinheim

[18] B. J. Melde, S. L. Burkett, T. Xu, J. T. Goldbach, T. P. Russell, *Chem. Mater.* **2005**, *17*, 4743.
[19] C. Jinan, W. Dong, F. Xiangning, J. M. Buriak, *Nat. Nanotechnol.* **2007**, *2*, 500.
[20] J. Spatz, S. Mossmer, M. Moller, M. Kocher, D. Neher, G. Wegner, *Adv. Mater.* **1998**, *10*, 473.
[21] D. H. Kim, S. H. Kim, K. Lavery, T. P. Russell, *Nano Lett.* **2004**, *4*, 1841.
[22] P. Soojin, W. Jia-Yu, K. Bokyung, T. P. Russell, *Nano Lett.* **2008**, *8*, 1667.
[23] W. van Zoelen, A. H. G. Vlooswijk, A. Ferri, A. M. Andringa, B. Noheda, G. ten Brinke, *Chem. Mater.* **2009**, *21*, 4719.
[24] W. A. Lopes, H. M. Jaeger, *Nature* **2001**, *414*, 735.
[25] R. H. A. Ras, M. Kemell, J. de Wit, M. Ritala, G. ten Brinke, M. Leskela, O. Ikkala, *Adv. Mater.* **2007**, *19*, 102.
[26] Y. Wang, Y. Qin, A. Berger, E. Yau, C. C. He, L. B. Zhang, U. Gosele, M. Knez, M. Steinhart, *Adv. Mater.* **2009**, *21*, 2763.
[27] M. Leskela, M. Ritala, *Angew. Chem. Int. Ed.* **2003**, *42*, 5548.
[28] R. L. Puurunen, *J. Appl. Phys.* **2005**, *97*, 52.
[29] S. M. George, *Chem. Rev.* **2010**, *110*, 111.
[30] Q. Peng, X. Y. Sun, J. C. Spagnola, G. K. Hyde, R. J. Spontak, G. N. Parsons, *Nano Lett.* **2007**, *7*, 719.
[31] M. Knez, K. Niesch, L. Niinisto, *Adv. Mater.* **2007**, *19*, 3425.
[32] J. D. Smith, *J. Organomet. Chem.* **1977**, *130*, 303.
[33] X. Assfeld, J. Garcia, J. I. Garcia, J. A. Mayoral, M. G. Proietti, M. F. Ruizlopez, M. C. Sanchez, *J. Chem. Soc.-Chem. Commun.* **1994**, 2165.
[34] S. Shambayati, W. E. Crowe, S. L. Schreiber, *Angew. Chem. Int. Ed.* **1990**, *29*, 256.
[35] A. Sinha, D. W. Hess, C. L. Henderson, *J. Vac. Sci. Technol. B* **2006**, *24*, 2523.
[36] J. P. Spatz, A. Roescher, M. Moller, *Adv. Mater.* **1996**, *8*, 337.
[37] J. W. Elam, M. D. Groner, S. M. George, *Rev. Sci. Instrum.* **2002**, *73*, 2981.
[38] M. Kemell, M. Ritala, M. Leskela, R. Groenen, S. Lindfors, *Chem. Vapor Depos.* **2008**, *14*, 347.

© 2010 WILEY-VCH Verlag GmbH & Co. KGaA, Weinheim